BEILSTEIN JOURNAL OF NANOTECHNOLOGY

Luminescence of $Tb_3Al_5O_{12}$ phosphors co-doped with Ce^{3+}/Gd^{3+} for white light-emitting diodes

Yu-Guo Yang*[1,2], Lei Wei[1,2], Jian-Hua Xu[1,2], Hua-Jian Yu[1,2], Yan-Yan Hu[1,2], Hua-Di Zhang[1,2], Xu-Ping Wang[1,2], Bing Liu*[1,2], Cong Zhang[1,2] and Qing-Gang Li[1,3]

Full Research Paper

Open Access

Address:
[1]Advanced Materials Institute, Qilu University of Technology (Shandong Academy of Sciences), Jinan 250014, China, [2]Qilu University of Technology (Shandong Academy of Sciences), Advanced Materials Institute, Key Laboratory of Light Conversion Materials and Technology of Shandong Academy of Sciences, Jinan 250014, China and [3]Qilu University of Technology (Shandong Academy of Sciences), Advanced Materials Institute, Shandong Provincial Key Laboratory of High Strength Lightweight Metallic Materials, Jinan 250014, China

Email:
Yu-Guo Yang* - yangyuguo@sdas.org; Bing Liu* - liubing@sdas.org

* Corresponding author

Keywords:
luminescence; $Tb_3Al_5O_{12}:Ce^{3+}/Gd^{3+}$; white light-emitting diodes (WLEDs)

Beilstein J. Nanotechnol. **2019,** *10,* 1237–1242.
doi:10.3762/bjnano.10.123

Received: 19 February 2019
Accepted: 03 June 2019
Published: 14 June 2019

Associate Editor: P. Leiderer

© 2019 Yang et al.; licensee Beilstein-Institut.
License and terms: see end of document.

Abstract

$Tb_{2.96-x}Ce_{0.04}Gd_xAl_5O_{12}$ phosphors were synthesized through solid-state reactions. The influence of Gd^{3+} on the luminescence was investigated. Under the excitation at 460 nm, $Tb_{2.96}Ce_{0.04}Al_5O_{12}$ shows the characteristic emission band of Ce^{3+} with a peak wavelength at about 554 nm. After co-doping Gd^{3+} into $Tb_{2.96}Ce_{0.04}Al_5O_{12}$, the peak wavelength of the Ce^{3+} emission band shifts to longer wavelengths, which is induced by the increasing crystal field splitting. However, the Ce^{3+} emission intensity also decreases because the substitution of Tb^{3+} with Gd^{3+} causes lattice deformation and generates numerous structural and chemical defects. By comparing the light parameters of white light-emitting diodes (WLEDs) containing $Y_{2.96}Ce_{0.04}Al_5O_{12}$, $Tb_{2.96}Ce_{0.04}Al_5O_{12}$ and $Tb_{2.81}Ce_{0.04}Gd_{0.15}Al_5O_{12}$ phosphors, we can find that the WLED containing the $Tb_{2.81}Ce_{0.04}Gd_{0.15}Al_5O_{12}$ phosphor generates warmer light than the WLEDs containing $Y_{2.96}Ce_{0.04}Al_5O_{12}$ and $Tb_{2.96}Ce_{0.04}Al_5O_{12}$ phosphors. Moreover, the WLEDs fabricated by integrating a blue LED chip and Ce^{3+}/Gd^{3+}-co-doped $Tb_3Al_5O_{12}$ phosphors show outstanding colour stability when driven under different currents.

Introduction

Currently, the most popular fabrication model of white light-emitting diodes (WLEDs) is to combine blue chips with yellow $Y_3Al_5O_{12}:Ce^{3+}$ phosphors, which has the disadvantages of low colour-rendering index (CRI) and high correlated colour temperature (CCT) [1,2]. At the same time, this type of WLEDs has the advantages of long lifetime, eco-friendliness, high luminous

efficiency and low energy consumption, which helps to mitigate two serious issues in the world, namely ecological crisis and energy dilemma. As a result, various attempts have been made to address the shortcomings in this type of WLED. To date, two common methods are red-light compensation and the red-shift of Ce^{3+} emission band in $Y_3Al_5O_{12}$. Red-light compensation is generally achieved by adding a red-emission phosphor, such as Eu^{2+}-doped materials [3], materials doped with trivalent lanthanide ions (e.g., Eu^{3+} and Sm^{3+}) [4-8], Mn^{4+}-doped materials [9-12], or Ce^{3+}/Cr^{3+}-co-doped $Y_3Al_5O_{12}$ [13,14]. The red-shift of the Ce^{3+} emission band in $Y_3Al1_5O_{12}$ is achieved, in general, through ion substitution, such as Ca^{2+}–Mg^{2+}–Si^{4+} [15], Si^{4+}–N^{3-} [16,17], Mg^{2+}–Si^{4+}/Ge^{4+} [18-20], or Gd^{3+} [21,22].

$Tb_3Al_5O_{12}$ has a garnet structure similar to $Y_3Al_5O_{12}$. A series of doped $Tb_3Al_5O_{12}$ phosphors have been synthesized, such as $Tb_3Al_5O_{12}:Ce^{3+}$ [23-25], $Tb_3Al_5O_{12}:Ce^{3+}/Eu^{3+}$ [26], $Tb_3Al_5O_{12}:Eu^{3+}$ [27], and $Tb_3Al_5O_{12}:Ce^{3+}/Ga^{3+}$ [28]. The results show that $Tb_3Al_5O_{12}$ is also a good host for various ions and the luminescent properties could be tuned by co-doping different ions into the $Tb_3Al_5O_{12}$ host. The $Tb_3Al_5O_{12}:Ce^{3+}$ phosphor also shows a yellow emission band. But the emission wavelength is longer than that of the $Y_3Al_5O_{12}:Ce^{3+}$ phosphor because Tb^{3+} ions produce a stronger crystal field effect [23-25]. The longer emission wavelength of $Tb_3Al_5O_{12}:Ce^{3+}$ is more suitable for WLEDs used as indoor illumination than that of $Y_3Al_5O_{12}:Ce^{3+}$. It is known that the sensitivity of human eyes to red light decreases strongly as soon as the wavelength is longer than 611 nm [9]. We aimed to shift the emission wavelength of $Tb_3Al_5O_{12}:Ce^{3+}$ to a longer wavelength that is, however, still shorter than 611 nm. In this work, we report the synthesis and luminescence of a series of Ce^{3+}/Gd^{3+}-co-doped $Tb_3Al_5O_{12}$ phosphors. The effect of co-doping Gd^{3+} on the luminescence of $Tb_3Al_5O_{12}:Ce^{3+}$ was investigated. It is found that the co-doped Gd^{3+} leads to a red-shift of the $Tb_3Al_5O_{12}:Ce^{3+}$ emission.

Results and Discussion

The phase of the synthesized $Tb_{2.96-x}Ce_{0.04}Gd_xAl_5O_{12}$ phosphors was confirmed by using XRD analysis. As shown in Figure 1, the diffraction peaks of $Tb_{2.96-x}Ce_{0.04}Gd_xAl_5O_{12}$ (x = 0, 0.05, 0.10, 0.15, 0.20, and 0.25) phosphors are well in accordance with the JCPDs card no. 17-1735, meaning that Ce^{3+}/Gd^{3+} ions have been doped into the $Tb_3Al_5O_{12}$ host entirely and formed a solid solution. Moreover, the diffraction peaks shift to lower 2θ angles with increasing x values, which is induced by the substitution of Tb^{3+} with Ce^{3+}/Gd^{3+}. The ionic radii of Tb^{3+}, Ce^{3+} and Gd^{3+} are 1.040 Å (CN = 8), 1.143 Å (CN = 8) and 1.053 Å (CN = 8), respectively. Due to the same valence and similar ionic radii of Tb^{3+}, Ce^{3+}, and Gd^{3+}, Tb^{3+} ions are replaced by Ce^{3+} and Gd^{3+} ions in Ce^{3+}/Gd^{3+} co-doped $Tb_3Al_5O_{12}$ phosphors. The larger ionic radii of Ce^{3+} and Gd^{3+} lead to the increase of the cell volume, which induces the shifts to lower 2θ angles of the diffraction peaks.

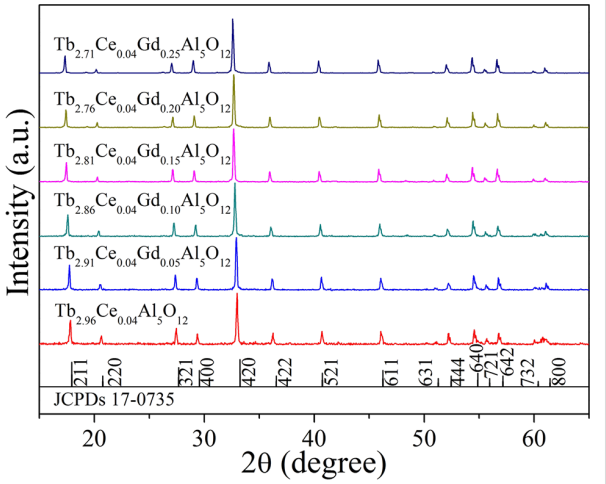

Figure 1: XRD patterns of $Tb_{2.96-x}Ce_{0.04}Gd_xAl_5O_{12}$ phosphors.

The excitation spectra of $Tb_{2.96-x}Ce_{0.04}Gd_xAl_5O_{12}$ phosphors, which show the excitation bands of Tb^{3+} and Ce^{3+} ions, is given in Figure 2. The excitation bands in the range of 250–300 nm with two excitation peaks at 275 and 286 nm correspond to the $4f^8 \rightarrow 4f^75d^1$ inter-configurational transitions of Tb^{3+} [28]. The weak excitation band with a peak at 375 nm is induced by the $^7F_6 \rightarrow {}^5D_3$ transition of Tb^{3+} [29]. Moreover, the $4f^8 \rightarrow 4f^75d^1$ transition of Tb^{3+} overlaps with the $4f \rightarrow 5d_2$ transition of Ce^{3+}, which results in the excitation band with a peak at 331 nm [22,26]. The strongest excitation band with a peak at 457 nm corresponds to the $4f \rightarrow 5d_1$ transition of Ce^{3+} [22]. It can be seen from Figure 2 that the excitation band corresponding to the $4f \rightarrow 5d_1$ transition of Ce^{3+} shifts to shorter wavelengths gradually with the increase of x, which is induced by the splitting of the Ce^{3+} 5d state. The increasing Gd^{3+} concentration leads to an intensified crystal field, which results in a stronger of splitting of the Ce^{3+} 5d state. As a result, the $4f \rightarrow 5d_1$ transition of Ce^{3+} shifts to shorter wavelengths, but the $4f \rightarrow 5d_2$ transition of Ce^{3+} shifts to longer wavelength. Herein, the shift of the $4f \rightarrow 5d_2$ transition of Ce^{3+} to longer wavelengths cannot be seen clearly because of its overlaps with the $4f^8 \rightarrow 4f^75d^1$ transition of Tb^{3+}.

Under excitation at 460 nm, $Tb_{2.96-x}Ce_{0.04}Gd_xAl_5O_{12}$ phosphors show the characteristic emission band of Ce^{3+}, as shown in Figure 3. One feature is the red-shift of the Ce^{3+} emission with increasing Gd^{3+} concentration and the other is the decrease of emission intensity with increasing Gd^{3+} concentration. The emission band of the $Tb_{2.96}Ce_{0.04}Al_5O_{12}$ phosphor peaks at

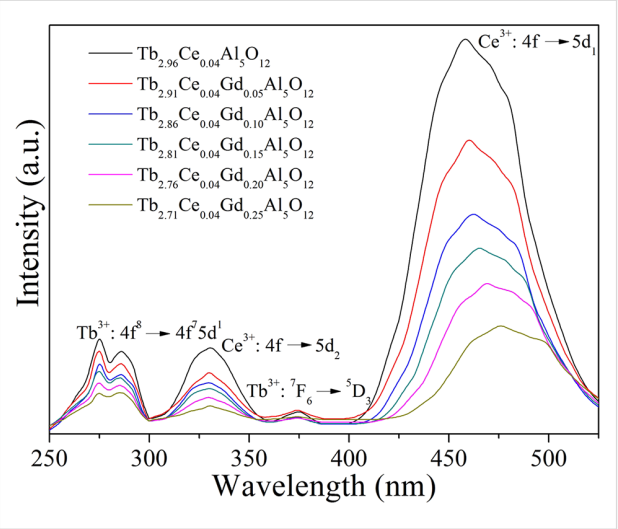

Figure 2: Excitation spectra of $Tb_{2.96-x}Ce_{0.04}Gd_xAl_5O_{12}$ phosphors.

about 554 nm. For the $Tb_{2.71}Ce_{0.04}Gd_{0.25}Al_5O_{12}$ phosphor, the peak wavelength of the emission band shifts to 610 nm. It is well known that the emission of Ce^{3+} depends on the crystal field splitting. The crystal field splitting can be calculated through the following equation:

$$10Dq = \frac{Ze^2r^4}{6R^5},$$

where $10Dq$ is the crystal field splitting parameter, Z is the anion charge, e is the electron charge, r is the radial distance of the d orbital from the nucleus, and R is the bond length [30,31]. Gd^{3+} has a larger ionic radius than of Tb^{3+}. As a result, the Ce^{3+}–O^{2-} bond length in $Tb_3Al_5O_{12}$:Ce^{3+}/Gd^{3+} decreases when Tb^{3+} ions are replaced by Gd^{3+} ions. The decrease of the Ce^{3+}–O^{2-} bond length results in an increase of the crystal field splitting, which in turn leads to the red-shift of the Ce^{3+} emission. This result is in accordance with the excitation spectra. Moreover, the substitution of Tb^{3+} with Gd^{3+} causes lattice deformation and generates numerous structural and chemical defects, which results in a decrease of the Ce^{3+} emission intensity [32]. The decay characteristics of the synthesized $Tb_{2.96-x}Ce_{0.04}Gd_xAl_5O_{12}$ phosphors were also investigated. Figure 4 gives the decay curves of $Tb_{2.96-x}Ce_{0.04}Gd_xAl_5O_{12}$ phosphors. The decay curves of the Ce^{3+} emission fit well with the second-order exponential formula

$$I(t) = A_1 \exp\left(-\frac{t}{\tau_1}\right) + A_2 \exp\left(-\frac{t}{\tau_2}\right),$$

where I is the emission intensity, A_1 and A_2 are constants, t is the time, and τ_1 and τ_2 are the rapid and the slow lifetime, respectively. The average lifetime (τ^*) can be calculated through

$$\tau^* = \frac{A_1\tau_1^2 + A_2\tau_2^2}{A_1\tau_1 + A_2\tau_2}.$$

The calculated τ^* values for $Tb_{2.96-x}Ce_{0.04}Gd_xAl_5O_{12}$ with x = 0, 0.05, 0.10, 0.15, 0.20, and 0.25 are 35.23, 31.46, 28.52, 26.37, 23.58 and 19.45 ns, respectively.

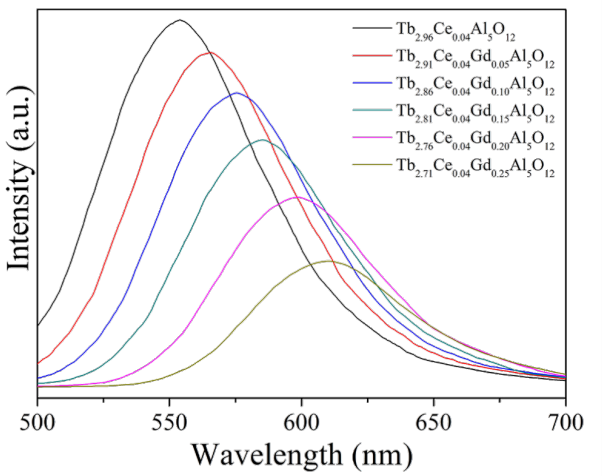

Figure 3: Emission spectra of $Tb_{2.96-x}Ce_{0.04}Gd_xAl_5O_{12}$ phosphors.

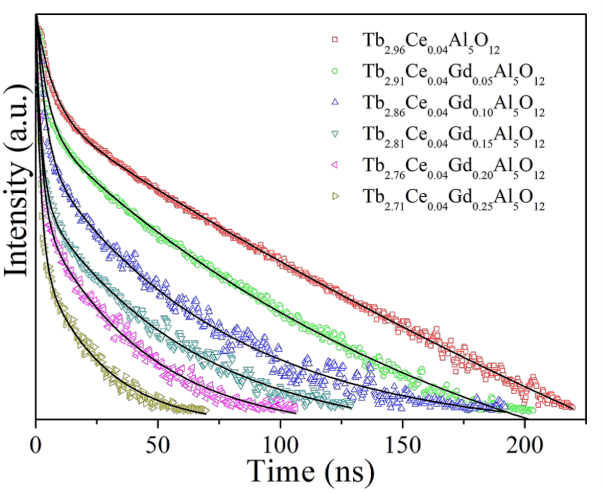

Figure 4: Decay curves of the Ce^{3+} emission from $Tb_{2.96-x}Ce_{0.04}Gd_xAl_5O_{12}$ phosphors.

The thermal stability of a phosphor is crucial for its applications in WLEDs. Thus, the emission spectra of a typical phosphor ($Tb_{2.81}Ce_{0.04}Gd_{0.15}Al_5O_{12}$) at different temperatures were measured and the results are shown in Figure 5. The emission intensity decreases continuously with the increasing temperature in the range of 300–540 K. As the temperature increases from 300 to 390 K, the emission intensity decreases by about 49%. Photon interaction plays an important role in thermal quenching, in which emission centres are thermally activated

and the energy is released through a nonradiative transition [31]. It is known that the probability of nonradiative transitions increases with increasing temperature. As a result, the emission intensity decreases with increasing temperature because of the higher number of nonradiative transitions.

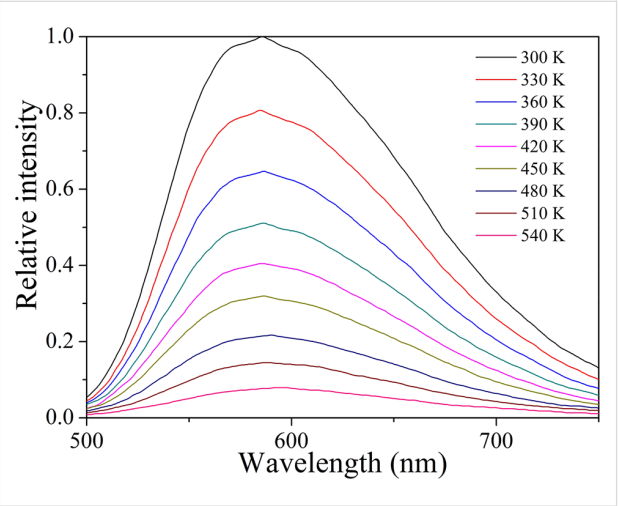

Figure 5: Emission spectra of $Tb_{2.81}Ce_{0.04}Gd_{0.15}Al_5O_{12}$ at different temperatures.

WLEDs were fabricated by combining a blue LED chip (460 nm) with $Y_{2.96}Ce_{0.04}Al_5O_{12}$, $Tb_{2.96}Ce_{0.04}Al_5O_{12}$ and $Tb_{2.81}Ce_{0.04}Gd_{0.15}Al_5O_{12}$ phosphors. The electroluminescence spectra under an operating current of 20 mA for the fabricated WLEDs are given in Figure 6. All of spectra consist of the blue excitation band of the LED chip and the emission band of the phosphor. The emission bands of the phosphors shift from 532 nm for $Y_{2.96}Ce_{0.04}Al_5O_{12}$ (Figure 6A) through 545 nm for $Tb_{2.96}Ce_{0.04}Al_5O_{12}$ (Figure 6B) to 589 nm for $Tb_{2.81}Ce_{0.04}Gd_{0.15}Al_5O_{12}$ (Figure 6C). The CIE chromaticity coordinates for the light from these three WLEDs are (0.325, 0.349), (0.368, 0.351), and (0.376, 0.338), respectively. The CCT values of the light from these three WLEDs are 5828, 4158, and 3767, respectively. These results suggest that $Tb_{2.81}Ce_{0.04}Gd_{0.15}Al_5O_{12}$ is a suitable phosphor for applications in WLEDs with low CCT for indoor lighting.

Generally, the colour stability of a LED device can be examined through measuring the colour deviation under different driving currents [33]. Figure 7 shows the electroluminescence spectra of a WLED containing the $Tb_{2.81}Ce_{0.04}Gd_{0.15}Al_5O_{12}$ phosphor under forward-bias currents of 5, 10, 20, 30, 40, and 50 mA. It can be seen that the intensity of the WLED increases with increasing current. Moreover, the shape and the peak of the bands corresponding to the LED chip and phosphor are consistent under different driving currents. This suggests the outstanding colour stability of the fabricated WLEDs.

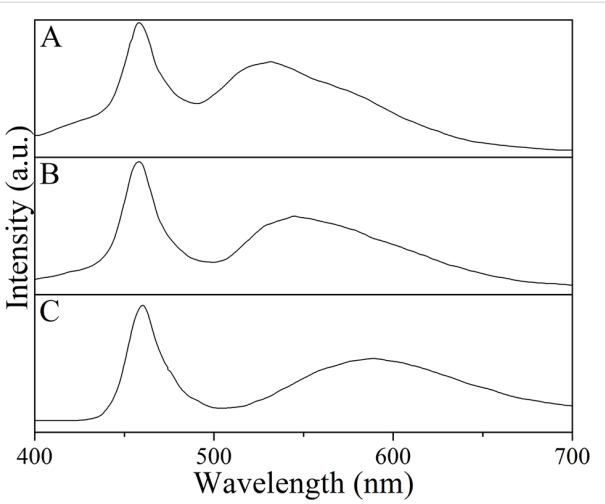

Figure 6: Electroluminescence spectra of WLEDs by combining blue LED chip with $Y_{2.96}Ce_{0.04}Al_5O_{12}$ (A), $Tb_{2.96}Ce_{0.04}Al_5O_{12}$ (B) and $Tb_{2.81}Ce_{0.04}Gd_{0.15}Al_5O_{12}$ (C) phosphors.

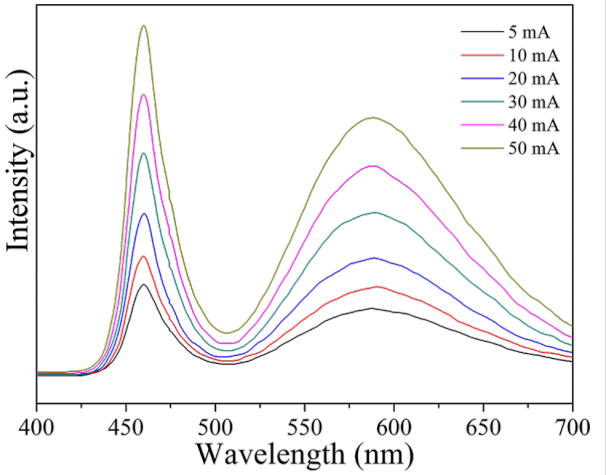

Figure 7: Electroluminescence spectra of a WLED with $Tb_{2.81}Ce_{0.04}Gd_{0.15}Al_5O_{12}$ phsphor under different forward-bias currents.

Conclusion

We synthesized a series of $Tb_{2.96-x}Ce_{0.04}Gd_xAl_5O_{12}$ phosphors through solid-state reactions. The doping with Ce^{3+}/Gd^{3+} ions does not lead to a phase change of the $Tb_3Al_5O_{12}$ host but induces a slight increase of cell volume. Under excitation at 460 nm, the $Tb_{2.96}Ce_{0.04}Al_5O_{12}$ phosphor shows the characteristic emission band of Ce^{3+} with a peak wavelength of about 554 nm. The co-doped Gd^{3+} ions lead to a red-shift of the Ce^{3+} emission band and the red-shifts become larger with increasing Gd^{3+} concentration. Due to the larger ionic radius of Gd^{3+} compared with Tb^{3+}, the substitution of Tb^{3+} with Gd^{3+} decreases the bond distance between Ce^{3+} and O^{2-}, which leads to an increase of crystal field splitting. The increasing crystal field splitting induces the red-shift of the Ce^{3+} emission. The longer

peak-wavelength of the Ce^{3+} emission for Gd^{3+} co-doped phosphors leads to a warmer light in WLEDs. The fabricated WLEDs by integrating a blue LED chip and the Ce^{3+}/Gd^{3+} co-doped $Tb_3Al_5O_{12}$ phosphors show outstanding colour stability when they are driven under different currents.

Experimental

A series of $Tb_{2.96-x}Ce_{0.04}Gd_xAl_5O_{12}$ (x = 0, 0.05, 0.10, 0.15, 0.20, and 0.25) phosphors were synthesized through solid-state reactions in a reduction atmosphere (5% H_2/95% N_2). Al_2O_3 (99.9%), Tb_4O_7 (99.9%), CeO_2 (99.99%) and Gd_2O_3 (99.95%) were used as starting materials. For the purpose of decreasing the reaction temperature, 4 wt % H_3BO_3 (99.5%) was added as flux. In a typical synthesis, we firstly weighted the raw materials according to stoichiometric ratios. Then, the raw materials were mixed in an agate mortar by grinding for 30 min and the mixture was calcined at 1350 °C for 5 h in an alumina crucible. Finally, the product was collected and reground after the temperature decreased to room temperature.

The X-ray diffraction (XRD) measurements were performed on a Rigaku D/max-RA X-ray diffractometer using Cu Kα radiation (λ = 1.5406 Å) with the experimental parameters of 40 kV, 30 mA and 2°/min. The measurements of excitation, emission, temperature-dependence of emission and decay curves were carried out in an Edinburgh Instrument FLS920 spectrophotometer equipped with a 450 W xenon lamp as the excitation source. The measurements were spectrally corrected. The samples were heated to a certain temperature and kept at this temperature for 5 min by using a temperature controller. The rate of temperature increase was less than 1 °C/ min and the temperature deviation was less than 0.1 °C.

Acknowledgements

This work was supported by the General Program of National Natural Science Foundation of China (51672164 and 51772172); Major Scientific and Technological Innovation Project in Shandong (2017CXGC0414 and 2018CXGC0412); Natural Science Foundation of Shandong Province (ZR2016EMM12, ZR2017MEM016, ZR2017BEM043, ZR2018BEM023 and ZR2018PEM006); Youth Foundation of Shandong Academy of Sciences (2018QN0033).

References

1. Sheu, J. K.; Chang, S. J.; Kuo, C. H.; Su, Y. K.; Wu, L. W.; Lin, Y. C.; Lai, W. C.; Tsai, J. M.; Chi, G. C.; Wu, R. K. *IEEE Photonics Technol. Lett.* **2003,** *15,* 18–20. doi:10.1109/lpt.2002.805852
2. Yang, Y.; Li, J.; Liu, B.; Zhang, Y.; Lv, X.; Wei, L.; Wang, X.; Xu, J.; Yu, H.; Hu, Y.; Zhang, H.; Ma, L.; Wang, J. *Chem. Phys. Lett.* **2017,** *685,* 89–94. doi:10.1016/j.cplett.2017.07.042
3. Pust, P.; Weiler, V.; Hecht, C.; Tücks, A.; Wochnik, A. S.; Henß, A.-K.; Wiechert, D.; Scheu, C.; Schmidt, P. J.; Schnick, W. *Nat. Mater.* **2014,** *13,* 891–896. doi:10.1038/nmat4012
4. Xia, Z.; Chen, D. *J. Am. Ceram. Soc.* **2010,** *93,* 1397–1401. doi:10.1111/j.1551-2916.2009.03574.x
5. He, Z.; Sun, X.-Y.; Teng, J.-X.; Gu, X. *J. Mater. Sci.: Mater. Electron.* **2018,** *29,* 8153–8157. doi:10.1007/s10854-018-8820-y
6. Liu, B.; Yang, Y.; Wang, X. *Nanosci. Nanotechnol. Lett.* **2013,** *5,* 1298–1301. doi:10.1166/nnl.2013.1687
7. Yang, Y. *Mater. Sci. Eng., B* **2013,** *178,* 807–810. doi:10.1016/j.mseb.2013.03.017
8. Yang, Y.; Wang, X.; Liu, B. *Nano* **2014,** *9,* 1450008. doi:10.1142/s1793292014500088
9. Du, M. H. *J. Mater. Chem. C* **2014,** *2,* 2475–2481. doi:10.1039/c4tc00031e
10. Li, J.; Yan, J.; Wen, D.; Khan, W. U.; Shi, J.; Wu, M.; Su, Q.; Tanner, P. A. *J. Mater. Chem. C* **2016,** *4,* 8611–8623. doi:10.1039/c6tc02695h
11. Chen, D.; Zhou, Y.; Xu, W.; Zhong, J.; Ji, Z.; Xiang, W. *J. Mater. Chem. C* **2016,** *4,* 1704–1712. doi:10.1039/c5tc04133c
12. Chen, Y.; Wu, K.; He, J.; Tang, Z.; Shi, J.; Xu, Y.; Liu, Z.-Q. *J. Mater. Chem. C* **2017,** *5,* 8828–8835. doi:10.1039/c7tc02514a
13. Ma, R.; Ma, C.; Zhang, J.; Long, J.; Wen, Z.; Yuan, X.; Cao, Y. *Opt. Mater. Express* **2017,** *7,* 454. doi:10.1364/ome.7.000454
14. Wu, Y.; Chi, Z.; He, T. *J. Mater. Sci.: Mater. Electron.* **2017,** *28,* 14591–14595. doi:10.1007/s10854-017-7323-6
15. Gorbenko, V.; Zorenko, T.; Witkiewicz, S.; Paprocki, K.; Iskaliyeva, A.; Kaczmarek, A. M.; Van Deun, R.; Khaidukov, M. N.; Batentschuk, M.; Zorenko, Y. *J. Lumin.* **2018,** *199,* 245–250. doi:10.1016/j.jlumin.2018.03.058
16. Setlur, A. A.; Heward, W. J.; Hannah, M. E.; Happek, U. *Chem. Mater.* **2008,** *20,* 6277–6283. doi:10.1021/cm801732d
17. Zhong, J.; Zhao, W.; Zhuang, W.; Du, F.; Zhou, Y.; Yu, Y.; Wang, L. *J. Alloys Compd.* **2017,** *726,* 658–663. doi:10.1016/j.jallcom.2017.08.023
18. Maniquiz, M. C.; Jung, K. Y. *ECS Trans.* **2010,** *28* (3), 175–182. doi:10.1149/1.3367224
19. Shang, M.; Fan, J.; Lian, H.; Zhang, Y.; Geng, D.; Lin, J. *Inorg. Chem.* **2014,** *53,* 7748–7755. doi:10.1021/ic501063j
20. Jiang, L.; Zhang, X.; Tang, H.; Zhu, S.; Li, Q.; Zhang, W.; Mi, X.; Lu, L.; Liu, X. *Mater. Res. Bull.* **2018,** *98,* 180–186. doi:10.1016/j.materresbull.2017.10.019
21. Shen, C.; Zhong, C.; Ming, J. *J. Exp. Nanosci.* **2013,** *8,* 54–60. doi:10.1080/17458080.2011.559589
22. Chen, L.; Chen, X.; Liu, F.; Chen, H.; Wang, H.; Zhao, E.; Jiang, Y.; Chan, T.-S.; Wang, C.-H.; Zhang, W.; Wang, Y.; Chen, S. *Sci. Rep.* **2015,** *5,* 11514. doi:10.1038/srep11514
23. Meng, Q.; Liu, Y.; Fu, Y.; Zu, Y.; Zhou, Z. *J. Mol. Struct.* **2018,** *1151,* 112–116. doi:10.1016/j.molstruc.2017.09.037
24. Onishi, Y.; Nakamura, T.; Adachi, S. *J. Lumin.* **2017,** *192,* 720–727. doi:10.1016/j.jlumin.2017.07.056
25. Choi, T. Y.; Song, Y. H.; Lee, H. R.; Senthil, K.; Masaki, T.; Yoon, D. H. *Mater. Sci. Eng., B* **2012,** *177,* 500–503. doi:10.1016/j.mseb.2011.10.005
26. Nazarov, M.; Noh, D. Y.; Sohn, J.; Yoon, C. *Opt. Mater.* **2008,** *30,* 1387–1392. doi:10.1016/j.optmat.2007.07.005
27. Onishi, Y.; Nakamura, T.; Sone, H.; Adachi, S. *J. Lumin.* **2018,** *197,* 242–247. doi:10.1016/j.jlumin.2018.01.043

28. Bi, J.; Wang, X.; Molokeev, M. S.; Zhu, Q.; Li, X.; Chen, J.; Sun, X.; Kim, B.-N.; Li, J.-G. *Ceram. Int.* **2018,** *44,* 8684–8690. doi:10.1016/j.ceramint.2018.02.104
29. Zorenko, Y.; Gorbenko, V.; Voznyak, T.; Zorenko, T.; Kuklinski, B.; Turos-Matysyak, R.; Grinberg, M. *Opt. Spectrosc.* **2009,** *106,* 365–374. doi:10.1134/s0030400x09030102
30. Robertson, J. M.; Tol, M. W. V.; Smits, W. H.; Heynen, J. P. H. *Philips J. Res.* **1981,** *36,* 15–30.
31. Zhang, H.; Chen, Y.; Zhu, X.; Zhou, H.; Yao, Y.; Li, X. *J. Lumin.* **2019,** *207,* 477–481. doi:10.1016/j.jlumin.2018.11.057
32. He, X.; Liu, X.; You, C.; Zhang, Y.; Li, R.; Yu, R. *J. Mater. Chem. C* **2016,** *4,* 10691–10700. doi:10.1039/c6tc02763f
33. Zhong, J.; Chen, D.; Zhou, Y.; Wan, Z.; Ding, M.; Bai, W.; Ji, Z. *Dalton Trans.* **2016,** *45,* 4762–4770. doi:10.1039/c5dt04909a

License and Terms

This is an Open Access article under the terms of the Creative Commons Attribution License (http://creativecommons.org/licenses/by/4.0). Please note that the reuse, redistribution and reproduction in particular requires that the authors and source are credited.

The license is subject to the *Beilstein Journal of Nanotechnology* terms and conditions: (https://www.beilstein-journals.org/bjnano)

The definitive version of this article is the electronic one which can be found at: doi:10.3762/bjnano.10.123